

# Radiation tests on erbium-doped garnet crystals for spaceborne CH<sub>4</sub>-Lidar applications

Ansgar Meissner, Martin Kreidler, Mirosław Cubera, Philipp Kucirek, Bastian Gronloh, Dominik Esser, Marco Höfer, Hans-Dieter Hoffmann,  
Fraunhofer Institute for Laser Technology, Steinbachstr. 15, 52074 Aachen, Germany

## ABSTRACT

A test campaign for assessing the radiation hardness of different Erbium-doped garnet crystals including Er:YAG and a compositionally tuned Er:YAG/Er:LuAG mixed garnet is reported. Tests with proton and gamma radiation have been performed with parameters mimicking a 3-year low-earth-orbit satellite mission like MERLIN or ADM-Aeolus. For each test sample broadband transmission spectra in the wavelength range of 500 nm – 1700 nm and characteristic laser curves from a test laser oscillator have been measured. Radiation-induced losses have been calculated from the obtained data. The results indicate that gamma radiation is the dominant loss source with about 0.5 %/cm radiation-induced losses for the nominal dose of the chosen mission scenario.

**Keywords:** laser crystals, Er:YAG, radiation testing, solid-state-laser, compositional tuning

## 1. INTRODUCTION

Methane (CH<sub>4</sub>) is one of the two greenhouse gases with the largest influence (measured as radiative forcing) on the IR-radiation budget of the Earth [1]. However, there is to date no working measurement system which can detect CH<sub>4</sub> abundances in the atmosphere on a global and long-term scale at any time of the day and under different weather conditions. The French-German mission Merlin (“Methane Remote Sensing LIDAR Mission”) is set to fill this gap in order to provide long-term data on global sources and sinks for CH<sub>4</sub>. It will consist of an active Integrated Path Differential Absorption Lidar Instrument [2] which will be operated on a satellite in low earth orbit (LEO) with about 450 km above the Earth’s surface. The differential absorption Lidar method requires a laser beam source which provides single-frequency laser pulses with pulse durations in the ns-regime and repetition rates between 10 and 100 Hz at specific wavelengths which are tuned to an absorption line of the target molecule, i.e. 1645.6 nm for CH<sub>4</sub> in the Merlin mission [3].

The traditional way to achieve such specific wavelength is deploying one or more optical-parametric stages with single-frequency pulsed pump lasers and single-frequency seed lasers. This also is the baseline for the Merlin mission [4]. An alternative solution is direct generation of the desired wavelength in a pulsed laser oscillator with an Erbium-doped crystal as the active medium. Direct generation of the laser pulses with the detection wavelength potentially provides lower complexity, higher efficiency and better spectral purity than the traditional way [5].

Er:YAG’s emission cross section has a maximum at a slightly short wavelength (1644.9 nm) but can be tuned by changing the crystal’s composition, e.g. by introducing Lutetium in the crystal lattice (compositional tuning [6]). This has been shown before for the Merlin wavelengths with Erbium-doped crystals. A laser oscillator providing laser radiation with suitable optical (especially spectral) properties has been reported [7]. If such a laser beam source is to be operated in Earth orbit, the radiation hardness of the laser crystal as the key component needs to be proven.

Literature on radiation tests of Er-doped garnet crystals report a significant effect of gamma radiation on transmission in the visible range and on laser properties of a flashlamp-pumped laser at

a wavelength of 2.94  $\mu\text{m}$ . Gamma irradiation with a dose in the krad-range significantly increases the output energy of a flashlamp-pumped laser, because induced color centers augment the absorption of the spectrally broad pump light [8].

Systematic studies of radiation effects on laser crystals with a space-application scenario have been reported for Nd-doped YAG and YLF crystals. It was found that both gamma and proton radiation cause significant losses in the visible and near-UV spectral region in Nd:YAG and Nd:YLF and that Cr-codoping of Nd:YAG increases radiation hardness [9].

To the best of our knowledge there are no reports in literature on systematic gamma and proton radiation tests with Er-doped YAG single crystals for space application in the 1.6  $\mu\text{m}$  spectral region. Also, while there are hints that Ce-codoping increases radiation hardness in Nd:YAG and Nd:YLF in a similar way as does Cr-codoping [10], the radiation hardening effect of Ce-codoping in Er:YAG has not been reported, yet.

## 2. TEST SAMPLES

Three different types of Erbium-doped host crystals are tested: Er:YAG, Er:YLuAG and Er,Ce:YLuAG. Here, Er:YLuAG denotes an Erbium-doped YAG/LuAG mixed garnet crystal with 4 % Lutetium content. The Er,Ce:YLuAG crystal has the same Lutetium content and is additionally co-doped with 0.1 at-% of Cerium. The doping of Erbium is 0.5 at-% in all cases. Doping levels are stated with respect to the Yttrium site.

All test samples have a physical length of 20 mm and are anti-reflection coated for 1532 nm and 1645 nm on both optical facets. The Er:YAG and Er,Ce:YLuAG samples are rods with a circular facet with a diameter of 2.5 mm. The barrel surfaces are fine-ground. The Er:YLuAG samples have a quadratic facet with an edge length of 2.5 mm. Its side surfaces are also fine-ground.

For Er:YLuAG and Er,Ce:YLuAG six individual test samples each are available for the tests, three of which are used for the proton test campaign and for the gamma test campaign, respectively. Of these three samples for each test campaign, one sample serves as a reference sample and is not irradiated, one sample is irradiated with the nominal dose derived from the mission scenario and one sample is irradiated with a ten times higher dose in order to allow for measuring radiation-induced losses even if they are small.

For Er:YAG, only four individual test samples are available. Therefore, tests with the nominal dose are not performed. Only the tenfold dose is tested.

## 3. TEST METHOD

The space mission scenario for the performed radiation tests is an earth observation mission from a low Earth orbit (about 450 km above the surface of the Earth) with duration of three years. In this orbit the relevant ionizing radiation types are gamma photons and protons, as the exposure to low-energy electron radiation at the poles are largely reduced with a reasonable thickness of metal shielding. Thus, in this test campaign test samples are exposed to gamma and proton radiation.

For testing the radiation effect on the test samples, two test setups are assembled. In a test laser oscillator each test sample is used as active medium, the laser characteristic curve is measured and its slope efficiency is measured. The radiation effect on the test sample is detected and measured as a change in slope efficiency after irradiation. Additionally, the transmission spectrum between 500 nm and 1700 nm is measured for each test sample. The radiation-induced losses are computed from the difference of the transmission spectra before and after irradiation.

Before irradiation, pre-irradiation tests (measurement of laser characteristic curve and transmission spectrum) are carried out for all of the test samples. For the irradiation the test samples are taken out of the test setups. After completion of the irradiation run post-irradiation tests are conducted. In order to minimize thermal healing of radiation-induced damages in the test samples the transmission spectra are measured before placing the test samples in the test laser oscillator. (Figure 1)

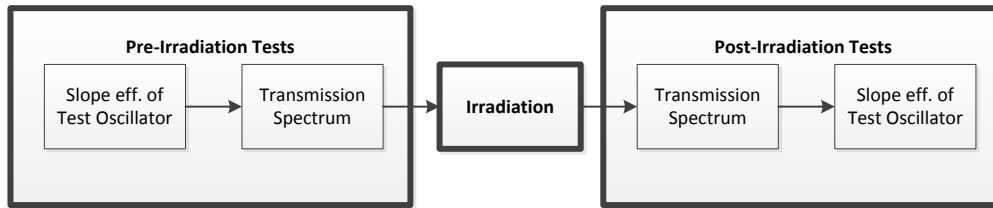


Figure 1: Sketch of the test flow for each individual test sample. This test flow is used both for proton and gamma radiation tests

In order to minimize the time delay between irradiation and post-irradiation tests (and thus minimize healing of radiation-induced damages) the whole test campaign (i.e. pre-irradiation tests, irradiation and post-irradiation tests) is conducted on-site at the irradiation source. The irradiation source for both campaigns (proton and gamma) is the Centre de Ressources du Cyclotron at the Catholic University of Louvain-La-Neuve in Belgium.

## 4. TEST SETUP

### 4.1 Test laser oscillator

The test laser oscillator (sketch in Figure 2) has a physical length of 120 mm and consists of a plane output coupler (OC) and a concave end mirror (EM) with a radius of curvature of  $r = 500$  mm. The transmission of the output coupler is  $T = 13\%$  and  $T = 5\%$  for the proton radiation tests and for the gamma radiation tests, respectively. The test samples (LC) are placed in the middle of the resonator between two plane dichroic pump mirrors (PM). The test samples are pumped with two fiber-coupled diode laser modules with a nominal emission wavelength of 1532 nm. The maximum optical power from each module is 25 W (cw). The delivery fibers have a core diameter of 400  $\mu\text{m}$  and numerical aperture of 0.22. The fiber end is imaged into the test samples with a two-lens telescope with a magnification of 1.5, resulting in a pump mode diameter of 600  $\mu\text{m}$  in the laser crystal.

The test samples are clamped with Indium-foil into copper heat sinks. These heat sinks are placed on a copper sub-mount. For the irradiation run the test samples are removed from the sub-mount in their individual heat sink. Alignment pins in the sub-mount allow for reproducible placement of the mounted test samples after irradiation. It is verified in advance that the remaining alignment error of the test laser oscillator is insignificant. The thermal contact between the heat sink and the sub-mount is established with heat-conductive paste. The temperature of the sub-mount set to 18  $^{\circ}\text{C}$  with a Peltier cooler and a PT-100 sensor in a closed-loop control unit. It is verified that the temperatures of the heat sink and the sub-mount are identical within an error range of 0.1  $^{\circ}\text{C}$ . Cooling of the “hot side” of the Peltier element is realized with a water-cooled cold plate made from copper. Heat-conductive paste is also used for the thermal coupling of the Peltier element with the copper parts.

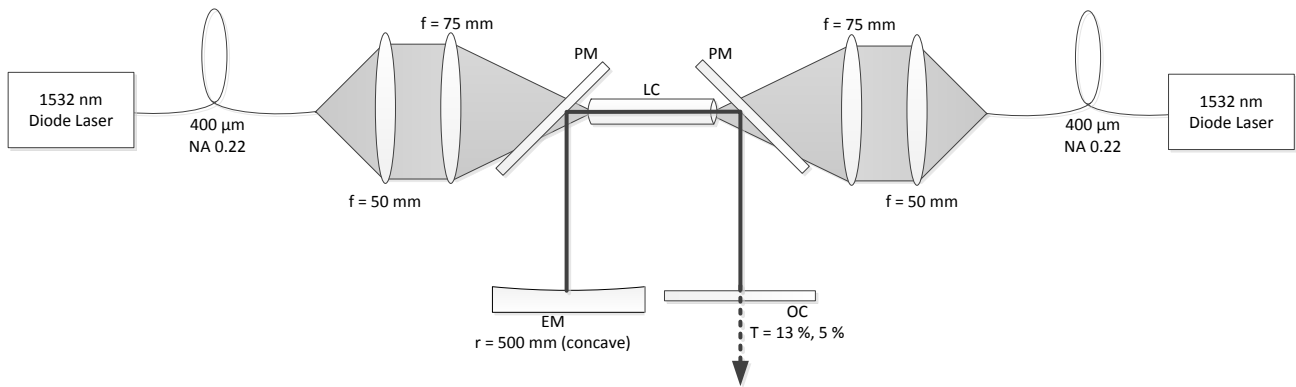


Figure 2: Schematic of the test laser oscillator. For the proton test campaign the output coupler's (OC) transmission was 13 %, for the gamma tests 5 %.

The laser output power behind the output coupler is measured with a thermopile power sensor Coherent LM-10 and a Coherent SSIM interface box.

#### 4.2 Transmission spectroscopy setup

The test samples are mounted in the same way as in the test laser oscillator. An identical sub-mount with Peltier-cooling is used, where the test samples mounted in the heat sinks can be reproducibly located in the spectroscopy setup. The test samples are illuminated with a fiber-coupled (400 μm core diameter, 0.22 NA) halogen lamp which emits a broad spectrum between 350 nm and 1800 nm. The white light from the fiber is collimated (beam diameter 1.6 mm) and launched into the test sample. The transmitted light is spatially homogenized in an integrating sphere and coupled into an optical spectrum analyser (Yokogawa AQ6315a) with another fiber with 400 μm core diameter and a numerical aperture of 0.22. (Figure 3)

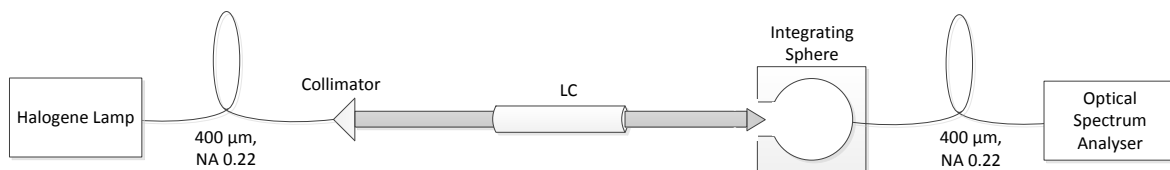


Figure 3: Schematic of the test setup for measuring transmission spectra. Collimated white light is launched into the test sample (LC) and the transmitted light is collected with an integrating sphere and a fiber and measured in an optical spectrum analyser (Yokogawa AQ6315a).

The temperature of the test sample mount is set and controlled to 18 °C. The spectra are measured with a spectral resolution of 2 nm and the highest sensitivity (“High3”). For the proton test campaign the sensitivity is set one level lower (“High2”) due to measurement time constraints.

## 5. GAMMA RADIATION TESTS

### 5.1 Test Parameters

In the given mission scenario with an assumed shielding of 4 mm aluminum the expected total ionizing dose is 2.1 krad(Si) [11]. This is therefore defined as the nominal dose for the gamma radiation tests. The tenfold dose is then 21 krad(Si), accordingly.

The dose rate is chosen to be 3.6 krad/hour which is the lowest specified dose rate in the “standard rate” window according to the ESA radiation testing standard ESCC22900 [12].

The gamma-radiation source at the Centre de Ressources du Cyclotron in Louvain-La-Neuve is a Co-60 source providing photon energies of 1.17 MeV and 1.33 MeV.

### 5.2 Test Results

The measured transmission spectra are smoothed using a Savitzky-Golay filter [13] with sub-set size of 100 points and quadratic polynomials in order to overcome significant noise in the raw data. The smoothing is not expected to affect the significance of the derived results because radiation-induced losses are spectrally broad.

From  $\log(I)_0(\lambda)$  and  $\log(I)_{irr}(\lambda)$ , the transmission spectra measured in logarithmic scale before and after the irradiation respectively, the radiation-induced losses in terms of an additional absorption coefficient

$$\Delta\alpha(\lambda) = \frac{1}{l_C} \ln \left( \frac{10^{\frac{\log(I)_0(\lambda)}{10}}}{10^{\frac{\log(I)_{irr}(\lambda)}{10}}} \right) \quad (1)$$

are computed for each individual test sample, where  $l_C$  is the physical length of the test sample. For all test samples, radiation-induced losses are stronger in the visible spectral range and decay with increasing wavelength. For wavelengths larger than about 1000 nm radiation-induced losses are smaller than the detection limit of about  $10^{-4}$  1/cm in this test campaign. (Figure 4)

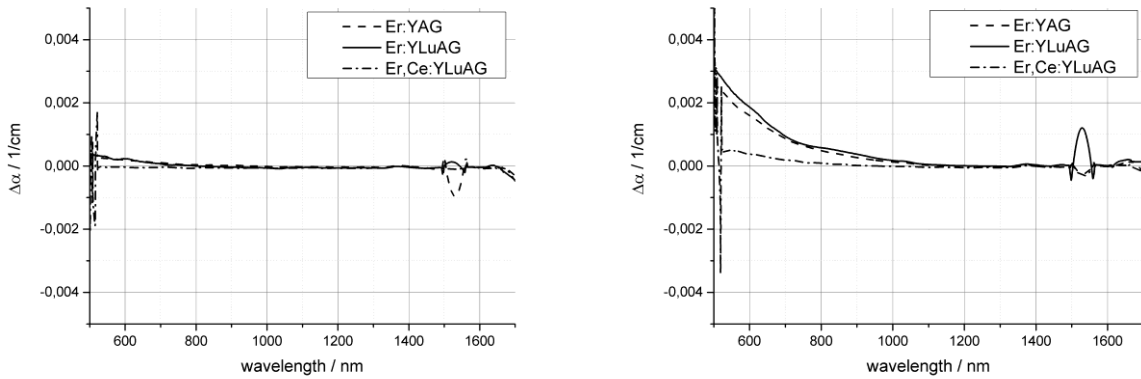


Figure 4. Radiation-induced loss spectra computed from the transmission spectra before and after irradiation. On the left-hand side the results are shown for the samples irradiated with the nominal gamma-dose of 2.1 krad(Si). On the right-hand side the spectra for the samples exposed to the tenfold dose 21 krad(Si) are shown. The curves are smoothed with a Savitzky-Golay filter with 100-points sub-sets and quadratic polynomials.

For test samples exposed to the nominal dose only radiation-induced losses of below 0.05 %/cm are measured at 500 nm. The test samples of Er:YAG and Er:YLuAG exhibit similar radiation-induced

losses, while for the Cer-codoped samples no radiation-induced losses are measured after irradiation with the nominal dose. A strong disturbance is measured at a wavelength of 1532 nm, which is the pump wavelength of the test laser oscillator. The integrating sphere of the spectroscopy setup collected scattered pump light from the adjacent test laser oscillator. The same is observed to a lesser degree at the laser wavelength of 1645 nm. These structures in the spectra are therefore discarded. (Figure 4, left)

After exposure to the tenfold gamma dose the radiation-induced losses are larger by roughly an order of magnitude. The test samples of Er:YAG and Er:YLuAG exhibit radiation-induced losses of about 0.3 %/cm at 500 nm and decay towards detection limit at about 1000 nm. Again, Er:YAG and Er:YLuAG samples show similar results while the measured radiation-induced losses for the Cer-codoped sample is smaller by almost an order of magnitude (0.05 %/cm at 500 nm). (Figure 4, right) From the characteristic curves measured from the test laser oscillator with the test samples as active media before and after irradiation the slope efficiencies  $\eta_0$  and  $\eta_{irr}$  are derived by fitting a straight line to the measured data. The ratio of these efficiencies then is used to compute the radiation-induced losses at the laser wavelength 1645 nm in terms of an additional absorption coefficient

$$\Delta\alpha = \frac{1}{2 \cdot l_C} \left( \frac{\eta_0}{\eta_{irr}} - 1 \right) \cdot (T + L_0), \quad (2)$$

where  $T = 5 \%$  is the transmission of the output coupler and  $L_0 = 2 \%$  is the dissipative round-trip loss of the laser oscillator.

For all test samples and all radiation doses the slope efficiencies after irradiation is lower than before irradiation. The drop in slope efficiency is stronger for the tenfold dose, where it drops to about half of the original value for Er:YAG and Er:YLuAG. The test samples with Cer-codoping still have a significant drop in slope efficiency (from 21 % to 15 % for the tenfold dose), but it is much weaker than for the other two crystal compositions. (Figure5, Figure 6, Figure 7)

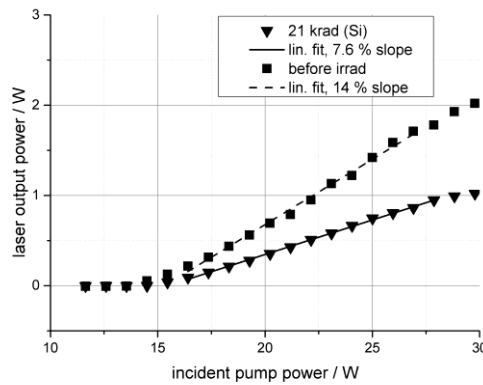


Figure 5. Laser characteristic curve for the Er:YAG test sample before and after irradiation with the tenfold gamma dose of 21 krad(Si).

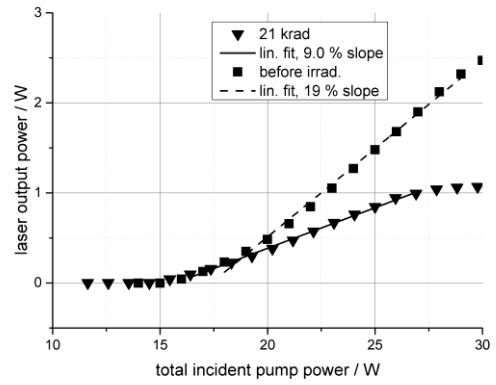
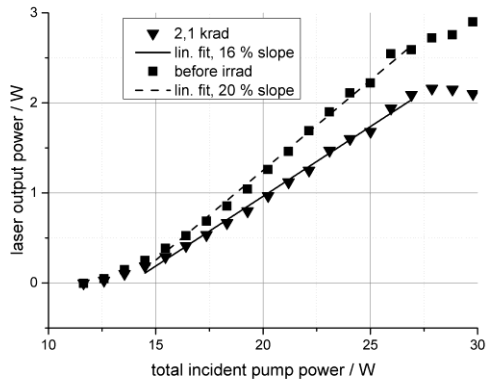


Figure 6. Laser characteristic curve for the Er:YLuAG test samples before and after irradiation. On the left hand side the results are shown for the sample exposed to the nominal dose, on the right-hand side for the tenfold dose.

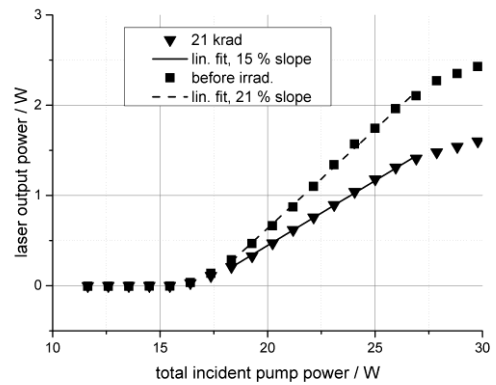
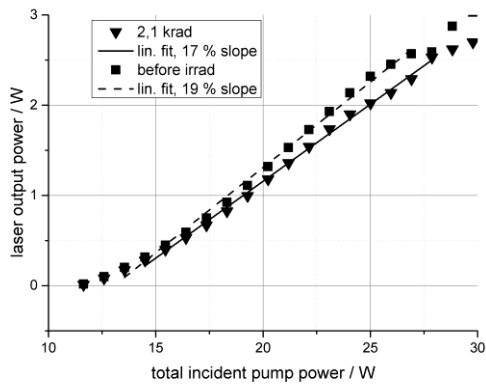


Figure 7. Laser characteristic curve for the Er,Ce:YLuAG test samples before and after irradiation. On the left hand side the results are shown for the sample exposed to the nominal dose, on the right-hand side for the tenfold dose.

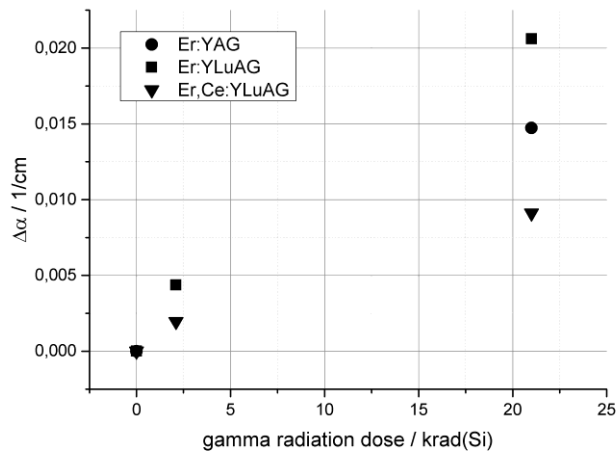


Figure 8. Measured radiation-induced losses of the different test samples as a function of the gamma radiation dose.

The laser characteristic curves show a slight roll-over towards 30 W of incident pump power, which is due to the spectral shift of the pump diodes with increasing driving current.

The radiation-induced losses computed from the characteristic curves using formula (2) are below 0.5 %/cm for the nominal dose. For the tenfold dose, Er:YLuAG exhibits the strongest losses with 2 %/cm and Er,Ce:YLuAG has the lowest losses with 1 %/cm. Again, the Ce-codoped test samples have significantly lower radiation-induced losses. (Figure 8)

### 5.3 Discussion

All measured test samples are considered sufficiently radiation hard with respect to gamma radiation, because even for the tenfold dose the radiation-induced losses do not exceed 2 %/cm. This value is smaller than typical transmissions of the output coupler (10 % - 20 %) for a q-switched laser oscillator for the MERLIN application scenario [7]. For such output coupling, the effect of the radiation induced losses on the laser performance is much less severe as it was observed here in the test campaign with  $T = 5\%$ . For the nominal dose of the mission scenario the losses are well below 1 %/cm and thus expected to be negligible for a laser oscillator with optimal output coupling. Ce-codoping is shown to increase radiation hardness of the Er:YLuAG crystal.

Although the radiation-induced losses measured with the test laser oscillator are well above detection limit of the spectroscopy setup, no radiation-induced losses are measured in the transmission spectroscopy tests in the relevant spectral region of 1.5  $\mu\text{m}$  to 1.7  $\mu\text{m}$ . This indicates that the loss mechanism in the laser experiments is not scattering or absorption of the laser light at 1645 nm but possibly a change in the dynamics of the electronic system. Further analysis is to be performed in order to identify the loss mechanism.

## 6. PROTON RADIATION TESTS

### 6.1 Test Parameters

In the given mission scenario a proton dose of 420 rad is expected. The cyclotron in Louvain-La-Neuve produces protons with particle energies up to 62 MeV. This proton particle energy is chosen for the proton test campaign, because at this particle energy the penetration depth of protons of 8.5 mm in YAG is roughly half of the length of the test samples, as is computed prior to the test campaign using the simulation tool SRIM [14][15][16] (c.f. Figure 9, solid line).

A proton fluence of  $3.3 \cdot 10^9$  protons/cm<sup>2</sup> for the given volume and mass density of the test samples is needed to achieve the nominal dose of 420 rad. The proton flux is set to  $1.1 \cdot 10^7$  protons/cm<sup>2</sup>/s. Also for the proton test campaign some test samples are exposed to the tenfold proton dose of 4200 rad.

### 6.2 Test Results

After the radiation test campaign the bulk absorption of the test samples is measured spatially resolved along the propagation direction of the protons with a photo-thermal common-path interferometer (PCI) at a test wavelength of 1030 nm [17][18][19].

The measurement results show strong absorption features at the front and rear surfaces of all the test samples. These features are used to refer the PCI-measurement axis to the absolute position of the test sample. At a penetration depth of 8.5 mm all of the test samples exhibit another strong absorption peak (Figure 9, dashed and dotted curves). This penetration depth was also predicted by the SRIM calculation (Figure 9, solid line). The level of absorption between the front surface and the absorption peak is significant and proton-dose dependent while the level of absorption behind the

absorption peak (towards the back surface of the samples) is low and only material dependent but not proton-dose dependent. It is deduced that the proton radiation has been absorbed in the test samples as expected. The radiation-induced absorption averaged over the test sample length (omitting the surface absorption structures) is 1.3 %/cm for Er:YLuAG, 1.0 %/cm for Er:YAG and 0.3 %/cm for Er,Ce:YLuAG. Due to lack of appropriate calibration samples, which are representative of the test samples, the absolute absorption values cannot be substantiated.

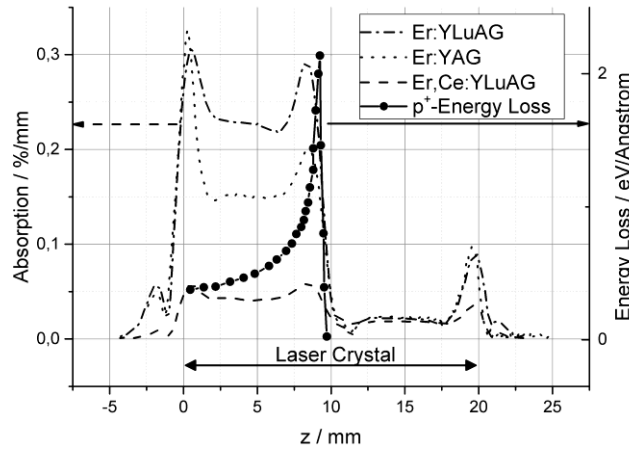


Figure 9. Results of the PCI-measurements at 1030 nm for the three test samples after exposure to the tenfold proton dose. The predicted proton energy deposition in the sample crystals derived from a SRIM calculation is also shown.

The evaluation method of the transmission spectra is identical to what is described in section 5.2 for the gamma radiation tests. The signal-to-noise ratio is lower here because the sensitivity of the optical spectrum analyzer had to be reduced.

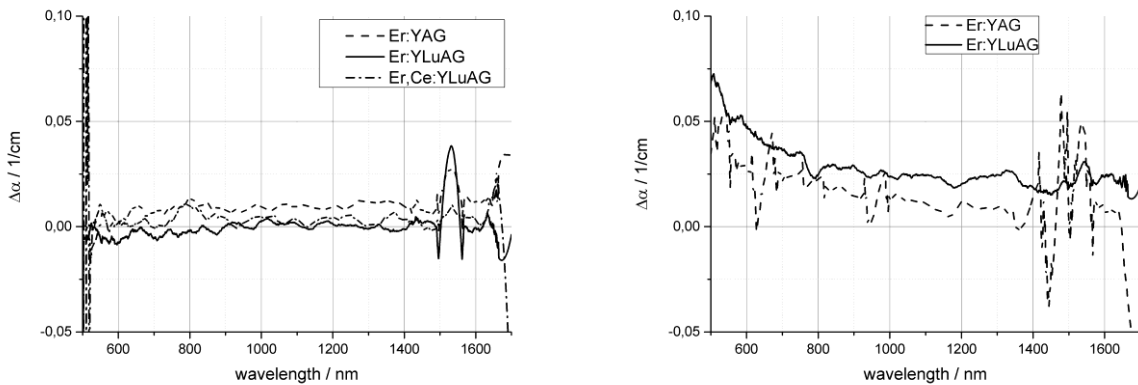


Figure 10. Radiation-induced loss spectra computed from the transmission spectra before and after irradiation. On the left-hand side the results are shown for the samples irradiated with the nominal proton-dose of 420 rad. On the right-hand side the spectra for the samples exposed to the tenfold dose 4200 rad are shown. The curves are smoothed with a Savitzky-Golay filter with 100-points sub-sets and quadratic polynomials.

Radiation-induced losses are below the (noise-dominated) detection limit of about 1 %/cm for all test samples exposed to the nominal proton dose (Figure 10, left). For the tenfold dose only the data from Er:YAG and Er:YLuAG are utilisable. An alignment problem with the Er,Ce:YLuAG test sample

prevents meaningful analysis of the spectral data for this test sample. For the other two test samples the radiation-induced losses show similar spectral dependence as in the gamma tests. Losses of 6 %/cm for Er:YLuAG and 5 %/cm are measured for 500 nm. The radiation-induced losses decay to about 2.5 %/cm at 1000 nm for Er:YLuAG and 1 %/cm for Er:YAG. (Figure 10, right)

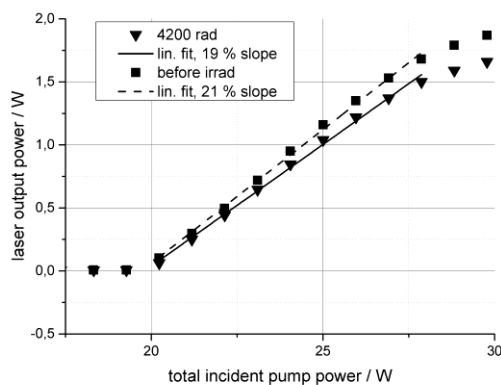


Figure 11. Laser characteristic curve for the Er:YAG test sample before and after irradiation with the tenfold proton dose of 4200 rad.

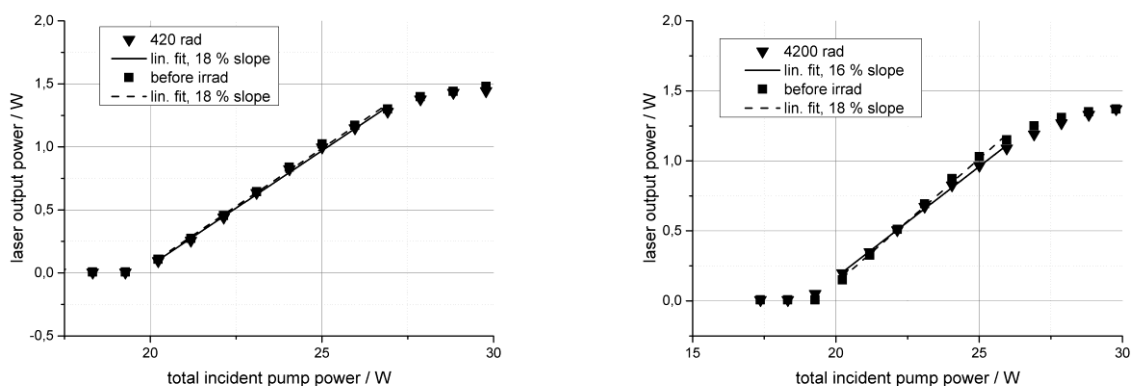


Figure 12. Laser characteristic curve for the Er:YLuAG test samples before and after irradiation. On the left hand side the results are shown for the sample exposed to the nominal dose, on the right-hand side for the tenfold dose.

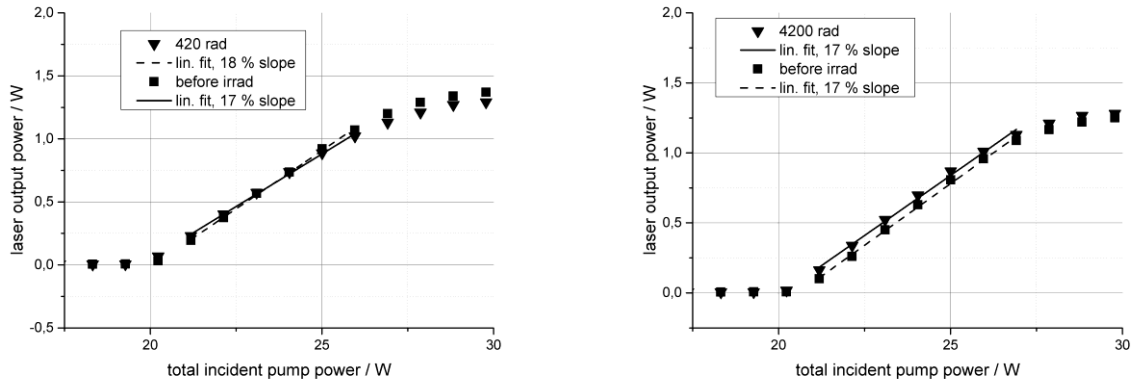


Figure 13. Laser characteristic curve for the Er,Ce:YLuAG test samples before and after irradiation. On the left hand side the results are shown for the sample exposed to the nominal dose, on the right-hand side for the tenfold dose.

The characteristic laser curves in the proton radiation test campaign are measured with an output coupler with a transmission of 13 %. The data are analysed in the same way as for the gamma radiation tests described in section 5.2. Changes in slope efficiency are marginal and only significant for the Er:YAG and Er:YLuAG test samples after exposure to the tenfold proton dose. For the nominal dose and all Er,Ce:YLuAG test samples no significant changes in slope efficiency after irradiation are observed. (Figure 11, Figure 12, Figure 13)

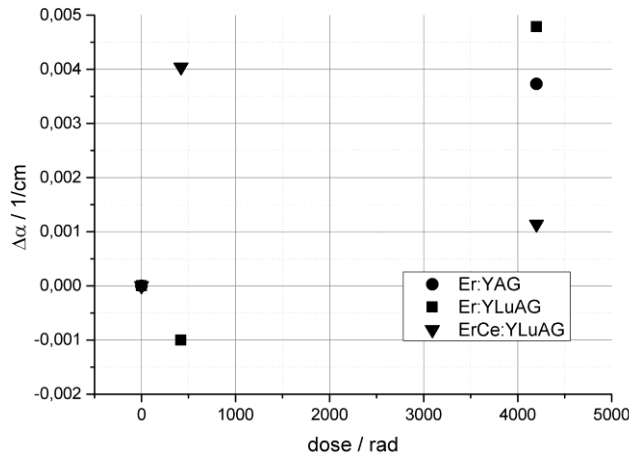


Figure 14. Measured radiation-induced losses of the different test samples as a function of the proton radiation dose.

The radiation-induced losses are computed from the slope efficiencies according to equation (2). They amount between 0.1 %/cm for Er,Ce:YLuAG and 0.5 %/cm for Er:YLuAG for the tenfold proton dose. In contrast to the results of the gamma radiation tests no clear dependence on proton dose is observed.

### 6.3 Discussion

Although not all of the results of the proton test campaign are consistent all measured radiation-induced losses are below 3 %/cm, even for the tenfold dose. Losses in this order of magnitude are

considered to be compensable in the laser oscillator by providing margin of pump power. Also, the effect of radiation-induced losses on the laser oscillator is much smaller than for the gamma radiation test campaign. This is attributed to the use of an output coupler with larger transmission ( $T = 13\%$  compared to  $T = 5\%$  in the setup of the gamma radiation campaign). This output coupling also causes larger errors on the measured radiation-induced losses in the laser experiments. A change of one percentage point in slope efficiency translates into a factor of two on the measured radiation-induced absorption. Taking this into account, the results of the laser oscillator tests, the transmission spectroscopy and the PCI-measurements are comparable.

Also with respect to proton radiation all used test samples are considered to be sufficiently radiation hard. Ce-codoping is shown to increase radiation hardness of the Er:YLuAG crystal.

## 7. CONCLUSION

Proton and gamma radiation tests of Er:YAG, Er:YLuAG and Er,Ce:YLuAG have been performed and radiation-induced losses have been measured in laser oscillator tests and transmission spectroscopy tests. All used test samples have been shown to be sufficiently radiation hard for usage as laser active medium in a satellite mission with duration of three years in a low Earth orbit. Losses induced by either gamma or proton radiation of the nominal dose are well below  $0.5\%/cm$ . For the tenfold dose, proton-induced losses are below  $5\%/cm$  in the visible and below  $2.5\%/cm$  in the IR spectral region. The radiation-induced losses of the Ce-codoped test samples are smaller by almost an order of magnitude compared to the singly-doped Er:YLuAG test samples. Thus, codoping with Cer has been shown to be a method for further radiation hardening of the Er-doped garnets, especially because the laser performance of the Ce-codoped samples are similar to that of the singly-doped samples.

Future work will be done in similar test campaigns for Tm- and Ho-doped laser crystals.

## 8. ACKNOWLEDGEMENTS

Part of this work was funded by the DLR RfM as a representative of the Federal Ministry of Economic Affairs and Energy under the contract number FKZ 50 EE 1222.

## REFERENCES

- [1] Solomon, S., Qin, D., Manning, M., Chen, Z., Marquis, M., Averyt, K.B., Tignor, M. and Miller, H.L. (eds.), "Contribution of Working Group I to the Fourth Assessment Report of the Intergovernmental Panel on Climate Change," Cambridge University Press (2007).
- [2] Spiers, G. D., Menzies, R. T., Tratt, D. M and Phillips, M., "The laser absorption spectrometer for carbon dioxide sink and source detection", Proceedings of the Second Annual Earth Science Technology Conference, NASA Earth Science Technology Office, Greenbelt (2002).
- [3] Kiemle, C., Quatrevalet, M., Ehret, G., Amediek, A., Fix, A., Wirth, M., "Sensitivity studies for a space-based methane lidar mission", Atmos. Meas. Tech. 4, 2195–2211 (2011).
- [4] Livrozet, M. J., Elsen, F., Wüppen, J., Löhring, J., Büdenbender, C., Fix, A., Jungbluth, B., Hoffmann, D., "Feasibility and performance study for a space-borne 1645 nm OPO for French-German satellite mission MERLIN", Proc. SPIE 8959, (2014).
- [5] Löhring, J., Meissner, A., Hoffmann, D., Fix, A., Ehret, G., Alpers, M., "Diode-pumped single-frequency-Nd:YGG-MOPA for water-vapor DIAL measurements: design, setup and performance," Appl Phys B 102, 917-935 (2011).

- [6] Barnes, N. P., Murray, K. E., Ertur, E. B., Walsh, B. M., Hutcheson, R. L., "Compositionally Tuned Solid State Lasers" in OSA TOPS on Advanced Solid-State Lasers, Payne, S. A., Pollock, C. (eds.), Optical Society of America, Washington, DC (1996).
- [7] Meissner, A., Kucirek, P., Li, J., Yang, S., Hofer, M., Hoffmann, D., "Simulations and experiments on resonantly-pumped single-frequency Erbium lasers at 1.6  $\mu\text{m}$ ", Proc. SPIE 8599, (2013).
- [8] Matkovskii, A. O., Sugak, D. Y., Durygin, A. N., Kaczmarek, S., Kopczynski, K., Mierczyk, Z., Frukacz, Z., Lukaszewicz, T., Shakhov, A. P., "Effect of ionizing radiation on optical and lasing properties of Y3Al5O12 single crystals doped with Nd, Er, Ho, Tm, Cr ions", Optical Materials 6, 353-358, (1996).
- [9] Rose, T. S., Hopkins, M. S., Fields, R. A., "Characterization and Control of Gamma and Proton Radiation Effects on the Performance of Nd:YAG and Nd:YLF Lasers", IEEE Journal of Quantum Electronics, Vol. 31, No. 9, 1593-1602, (1995).
- [10] Kaczmarek, S. et al., "Effect of increase of Ce<sup>3+</sup> ions content after gamma irradiation of Ce and Ce, Nd doped YAG single crystals," Biuletyn WAT, vol. 8, p. 93, (1996).
- [11] European Space Agency, "2.05 Microns Pulsed Holmium Laser for Atmospheric CO<sub>2</sub> Monitoring", Statement of Work, TEC-MME/2012/299, (2012).
- [12] European Space Agency, ESCC, "Total Dose Steady-State Irradiation – Test Method", ESCC Basic Specification No. 22900, (2010).
- [13] Savitzky, A. and Golay, M. J. E., "Smoothing and Differentiation of Data by Simplified Least Squares Procedures," Analytical Chemistry. 36, No. 8, 1627-1639, (1964), doi:10.1021/ac60214a04.
- [14] Ziegler, J. F., „James Ziegler - SRIM & TRIM,“ <www.srim.org.> (25 April 2013)
- [15] Biersack, J. P. and Haggmark, L., Nucl. Instr. and Meth., Nr. 174, p. 257, (1980).
- [16] Ziegler, J. F., "The Stopping Range of Ions in Matter", Pergamon Press, (1985).
- [17] Alexandrovski, A., "How it works," <http://www.stan-pts.com/howitworks.html> (14 February 2014).
- [18] Alexandrovski, A., Fejer, M., Markosyan, A., Route, R., "Photothermal commonpath interferometry (PCI): new developments," Proc. SPIE 7193 Solid State Lasers XVIII: Technology and Devices, 71930D (2009).
- [19] Zhuang, F., Jungbluth, B., Gronloh, B., Hoffmann, H., Zhang, G., "Dual-wavelength, continuous-wave Yb:YAG laser for high-resolution photothermal common-path interferometry," Appl. Opt. 52, 5171-5177 (2013).